International Journal of Nanomedicine

Dovepress
open access to scientific and medical research

Open Access Full Text Article

ORIGINAL RESEARCH

Carboxymethyl chitosan nanoparticles loaded with bioactive peptide OH-CATH30 benefit nonscar wound healing

This article was published in the following Dove Press journal:
International Journal of Nanomedicine

Tongyi Sun,[1] Bo Zhan,[2,3] Weifen Zhang,[2] Di Qin,[1] Guixue Xia,[2] Huijie Zhang,[1,3] Meiyu Peng,[4] Sheng-An Li,[3] Yun Zhang,[3] Yuanyuan Gao,[2] Wen-Hui Lee[1,3]

[1]Department of Bioengineering, School of Bioscience and Technology, Weifang Medical University, Weifang 261053, Shandong, China; [2]Department of Pharmaceutics, School of Pharmacy, Weifang Medical University, Weifang 261053, Shandong, China; [3]Key Laboratory of Bioactive Peptide of Yunnan Province/Key Laboratory of Animal Models and Human Disease Mechanisms of the Chinese Academy of Sciences, Kunming Institute of Zoology, Chinese Academy of Sciences, Kunming 650223, Yunnan, China; [4]Department of Immunology, School of Clinical Medicine, Weifang Medical University, Weifang 261053, Shandong, China

Background: Nonscar wound healing is a desirable treatment for cutaneous wounds worldwide. Peptide OH-CATH30 (OH30) from king cobra can selectively regulate the innate immunity and create an anti-inflammatory micro-environment which might benefit nonscar wound healing.

Purpose: To overcome the enzymatic digestion and control release of OH30, OH30 encapsulated in carboxymethyl chitosan nanoparticles (CMCS-OH30 NP) were prepared and their effects on wound healing were evaluated.

Methods: CMCS-OH30 NP were prepared by mild ionic gelation method and properties of the prepared CMCS-OH30 NP were determined by dynamic light scattering. Encapsulation efficiency, stability and release profile of OH30 from prepared CMCS-OH30 NP were determined by HPLC. Cytotoxicity, cell migration and cellular uptake of CMCS-OH30 NP were determined by conventional methods. The effects of prepared CMCS-OH30 NP on the wound healing was investigated by full-thickness excision animal models.

Results: The release of encapsulated OH30 from prepared CMCS-OH30 NP was maintained for at least 24 h in a controlled manner. CMCSOH30 NP enhanced the cell migration but had no effects on the metabolism and proliferation of keratinocytes. In the full-thickness excision animal models, the CMCS-OH30 NP treatment significantly accelerated the wound healing compared with CMCS or OH30 administration alone. Histopathological examination suggested that CMCS-OH30 NP promoted wound healing by enhancing the granulation tissue formation through the re-epithelialized and neovascularized composition. CMCS-OH30 NP induced a steady anti-inflammatory cytokine IL10 expression but downregulated the expressions of several pro-inflammatory cytokines.

Conclusion: The prepared biodegradable drug delivery system accelerates the healing and shows better prognosis because of the combined effects of OH30 released from the nanoparticles.

Keywords: wound healing, antimicrobial peptide, OH-CATH30, nanoparticles, skin destruction

Introduction

Skin scarring after trauma, surgery, burn, or sports injury frequently happens in humans and animals. Scarring is a worldwide major medical problem and often results in function loss, tissue movement restriction, and psychological adverse effects.[1] Unfortunately, the current treatments for skin scarring are empirical, unreliable, and unpredictable; no prescription drugs are available in clinic for the prevention or treatment of scarring.[2] Scarring is closely related to wound healing, a well-orchestrated process of replacing devitalized and missing cellular structures and tissue layers.[3] Wound healing is generally divided into four overlapping phases, namely, hemostasis, inflammation, migration and proliferation, and maturation.[4]

Evidence from scar-free healing in embryonic wounds and scar-forming healing in adult wounds in mammals suggests that the inflammation phase and the sterile microenvironment around the wound play an important role in the fate of wound healing.[5] Keeping an

Correspondence: Wen-Hui Lee
Kunming Institute of Zoology, Chinese Academy of Sciences, 32, East Jiaochan Road, Kunming 650223, Yunnan, China
Tel +86 871 6519 4279
Email leewh@mail.kiz.ac.cn

Yuanyuan Gao
School of Pharmacy, Weifang Medical University, Baotong Road, Weifang, Shandong Province 261053, China
Tel/fax +86 536 846 2067
Email yyg20062006@126.com

submit your manuscript | www.dovepress.com
Dovepress
http://dx.doi.org/10.2147/IJN.S156206

© 2018 Sun et al. This work is published and licensed by Dove Medical Press Limited. The full terms of this license are available at https://www.dovepress.com/terms.php and incorporate the Creative Commons Attribution – Non Commercial (unported, v3.0) License (http://creativecommons.org/licenses/by-nc/3.0/). By accessing the work you hereby accept the Terms. Non-commercial uses of the work are permitted without any further permission from Dove Medical Press Limited, provided the work is properly attributed. For permission for commercial use of this work, please see paragraphs 4.2 and 5 of our Terms (https://www.dovepress.com/terms.php).

anti-inflammatory and sterile microenvironment around the wound significantly helps nonscar wound healing.[6]

Antimicrobial peptides (AMPs) are short positively charged peptides found in various life forms from microorganisms to humans.[7] Most AMPs have the ability to directly kill microorganisms, whereas others indirectly act by modulating the host defense systems. Interestingly, many AMPs also have immune modulation activity apart from their bactericidal activity.[8] A few AMPs have been carrying clinical trials, human cathelicidin member LL-37 to promote the healing of venous leg ulcers[9] and PXL01, derived from human lactoferricin, to prevent postsurgical adhesion formation (NCT01022242) were conducted.[10,11]

We first reported that the cathelicidin family of AMPs exists in reptile species of *Naja atra*, *Bungarus fasciatus*, and *Ophiophagus hannah* snake species.[12] We focused on cathelicidin from king cobra (OH30) and revealed that this peptide has strong antibacterial activity against various bacteria in the presence of 1% NaCl. OH30 shows better bactericidal, weaker hemolytic to human erythrocytes, weaker cytotoxic on cultured human cells, and lower acute toxicity on mice than pexiganan, a 22 amino acid residue AMP derived from frog *Xenopus magainin* that already completed two clinical trials on Phase III for the treatment of infectious-related hard-to-heal diabetic foot ulcer.[13] Furthermore, OH30 significantly reduces the bacterial counts in a mouse thigh infection model. The mechanism of OH30 to protect the infected mouse in a bacteremia model is attributed to its inflammatory regulation activities.[14] OH30 exhibits an improved clinical effect of treating antibiotic-resistant *Pseudomonas aeruginosa* that induces rabbit keratitis.[15] Importantly, strong direct bactericidal activity and selective regulation of the expression of various chemokines and cytokines of OH30 are demonstrated to be responsible for protecting the animals from lethal sepsis.[16] Other investigations using reptile cathelicidins as the template also reveal that snake elapid cathelicidins can serve as model molecules for the development of antimicrobial drugs.[17]

In wound healing applications, chitosan (CS) is one of the widely used naturally based polymers. Carboxymethyl chitosan (CMCS) is a water-soluble CS derivative successfully used as biomaterials in both research and clinical applications. Due to their favorable biocompatibility, no antigenicity, moisture retention, specific bioadhesion, and antibacterial ability, CS and CMCS are regarded as attractive materials for wound healing agents.[18,19] Recently, they have also been applied as the polymer materials for the bioactive peptide delivery. Insulin was successfully encapsulated in CMCS nanocarriers under mild conditions and showed improvement in animal models.[20] Furthermore, the nanoparticles with positive surface charges are capable of ionic interaction with cell membranes carrying negative charges, which can accelerate their cellular internalization.[21] Thus, positive surface charged nanoparticles coated with CS and CMCS might be suitable to encapsulate peptide molecules, such as AMPs, for wound care application.

To take advantage of the immune regulatory of OH30 and CMCS NP as a good nanocarrier to decrease OH30 digestion by enzymes, we hypothesized that the administration of OH30 encapsulated in CMCS nanoparticles (CMCS-OH30 NP) might maintain a steady anti-inflammatory microenvironment to benefit wound healing because of the sustained release of OH30. Therefore, CMCS-OH30 NP inducing nonscar wound healing was investigated in the present study.

Materials and methods

Materials

CS [Mw = 12 kDa; the degree of deacetylation (DD) = 90%] was purchased from Sigma-Aldrich (St Louis, MO, USA). CMCS [Mw = 12 kDa, DD = 85%, the degree of substitution (DS): 90%] was synthesized and characterized as previously described.[22] OH30, FITC-labeled OH30, and Cy5-labeled OH30 (amino acid sequence, KFFKKLKNSVKKRAKKFFKKPRVIGVSIPF; purity ≥96%) were synthesized by GL Biochem (Shanghai, China). Phosphate-buffered saline (PBS, pH 7.4), 3-(4,5-dimethyl-2-tetrazolyl)-2,5-diphenyl-2H tetrazolium bromide (MTT), hematoxylin and eosin (H&E), and Masson's trichrome (MT) stain were purchased from Solarbio (Beijing, China). Fetal bovine serum (FBS), Calcein AM, and Hoechst 33258 were purchased from Thermo Fisher Scientific (Waltham, MA, USA).

Preparation and characterization of CMCS-OH30 NP

CMCS-OH30 NP were prepared according to the previously described ionic gelation method.[21] Briefly, the OH30 aqueous solution (1 mg/mL, pH 7.4), CMCS aqueous solution (1 mg/mL, pH 7.4), and CS acetic acid solution (1 mg/mL, pH 6.0) were separately prepared. OH30 and CMCS solutions were premixed for 30 min under magnetic stirring; the formed primary structure was termed as CMCS-OH30 PNP. CMCS-OH30 PNP is the primary core of the final nanoparticle formed first through the alternate adsorption of oppositely charged CMCS and OH30. CS solution was drop-wise added into the obtained CMCS:OH30 mixture at a proportion by weight (CS:CMCS:OH30 = 0.4:2:1) under constant stirring for 1 h until the formation of nanoparticles. CMCS-OH30 NP were collected via ultracentrifugation at 12,000 rpm at 4°C for 30 min and were washed with sterile ultrapure water

twice. The formed nanoparticles, after centrifugation, were then resuspended in distilled water using a probe sonication (pulse on, 3.0 s; pulse off, 2.0 s; 1 min/cycle; power 130 W) for storage and characterization.

The particle size distribution, zeta potential of vesicle, and OH30-loaded NP were determined by dynamic light scattering using a Malvern Nano-ZS 90 laser particle size analyzer (Malvern Instruments, Malvern, UK) at a detector angle of 90°, 670 nm, and temperature of 25°C. Morphology of CMCS-OH30 NP was examined by atomic force microscope (AFM, SPA-400, Seiko Instruments Inc., Qianye, Japan).[23]

Encapsulation efficiency (EE) and stability of OH30

The EE and drug loading efficiency (LE) of CMCS-OH30 NP were determined according to the method described.[23] Briefly, the free OH30 released from CMCS-OH30 NP in the supernatants was evaluated by high-performance liquid chromatography (HPLC) on a ZORBAX 300SB-C_{18} column (5 µm, 4.6 × 250 mm, Agilent, CA, USA); Waters 1525 HPLC system with Waters 2489 UV/Visible detector was used in the experiments. The gradient was first maintained for 5 min at 80% H_2O/0.1% $C_2HF_3O_2$ and 20% CH_3CN/0.1% $C_2HF_3O_2$, followed by 20 min at 60% H_2O/0.1% $C_2HF_3O_2$ and 40% CH_3CN/0.1% $C_2HF_3O_2$. The elution flow rate was 1 mL/min, and the quantity of released OH30 was calculated by comparing with the determined calibration curve. The EE and LE were calculated according to formulas (1) and (2):[24]

$$EE = \left(\frac{Wt - Wn}{Wt}\right) \times 100\%, \quad (1)$$

$$LE = \left(\frac{Wt - Wn}{Wm}\right) \times 100\%, \quad (2)$$

where Wt, Wn, and Wm refer to the weight of total OH30 used, OH30 nonencapsulated, and OH30 loaded NP, respectively (n = 6).

The CMCS-OH30 NP were stored at 4°C for 28 days. The physical stability of NP was evaluated by monitoring the particle size and zeta potential during the storage.[25]

In vitro study of drug release profile

To mimic clinical conditions, in vitro release behavior of OH30 from nanoparticles was determined in simulated wound fluid (SWF). The lyophilized CMCS-OH30 PNP and CMCS-OH30 NP were, respectively, dissolved in 10 mL of SWF in centrifuge tubes (maximum volume: 15 mL) under gentle shaking at 37°C. SWF consisted of 50% calf serum and 50% maximum recovery diluent (0.1% w/v peptone and 0.9% w/v sodium chloride).[26] The release systems were shaken at 50 rpm in a water bath at 37°C. At specific time intervals, the supernatant was obtained after centrifugation. The releasing media (1.0 mL) was removed and replaced by fresh SWF (1.0 mL). The OH30 released from nanoparticles was investigated by transmission electron microscopy (JEM-2100; JEOL, Akishima-shi, Japan). The concentration of OH30 released was determined by HPLC as described in the "Encapsulation efficiency (EE) and stability of OH30" section to calculate the cumulative OH30 release rate.

Antibacterial activity assays

The aliquots prepared at different time points of previous drug release steps were evaluated against *Escherichia coli* 25922 according to the method described.[27] Briefly, bacteria were incubated at 37°C in Luria–Bertani (LB) broth until exponential growth was observed. Equal volume (100 µL) of LB diluted bacteria at approximately 5×10^5 CFU/mL was incubated with the prepared OH30 NP aliquots for 30 min. Then, the mixtures were spread onto the LB agar plates and the changes in the viable bacterial counts were measured the following day (14–16 h).

Cytotoxicity assay

The human keratinocyte cell line HaCaT, human skin fibroblasts cell strain BJ fibroblasts, and *Mus musculus* macrophages RAW264.7 were purchased from Kunming Cell Bank of Type Culture Collection (Kunming Institute of Zoology, CAS). The cytotoxicity of the formulation was detected by conventional MTT cell viability assay as described.[25,28] Briefly, experimental cells were cultured in DMEM/F-12 (10% FBS) and were supplemented with L-glutamine and HEPES. Cells (3,000 cells/well, n = 5) were first seeded in 96-well plates (Corning Incorporated, Corning, NY, USA) and incubated at 37°C and 5% CO_2 for 24 h. The culture medium was subsequently replaced with 100 µL of fresh DMEM/F-12 containing various concentrations of OH30, CMCS NP, and CMCS-OH30 NP. After incubation for further 24 h, the cell viability assays were measured.

Cell migration assay

The ability of CMCS-OH30 NP to stimulate the migration of HaCaT cells was studied through a modified scratch assay method.[29] Ibidi culture inserts (Ibidi, Martinsried, DE, USA) were mounted on a 24-well plate (Corning Incorporated). HaCaT cells were seeded on both sides of the inserts (15,000 cells/side) and were incubated with 5% CO_2 at 37°C. After the cells reached 80% confluence, the inserts were removed from the wells and were washed with PBS to remove

the debris. A cell-free area (500 μm pseudo-"wound") was created. Different samples (50 μg/mL OH30, 50 μg/mL CMCS NP, 50 μg/mL CMCS-OH30 NP, and untreated control) were administered, and the cells were allowed to invade the cell-free area. Micrographs were captured at the beginning (0 h) and every 6 h for 24 h using Olympus IX71 microscopy (Olympus Corporation, Tokyo, Japan).

Cellular uptake study

RAW264.7 cells were cultured on glass-bottom cell culture dishes (inner diameter 35 mm) for 24 h to form a monolayer of interconnected cell layer. Cy5-labeled OH30 and CMCS-OH30 NP were separately suspended in culture medium to a final concentration of 50 μg/mL. Accordingly, free OH30 and CMCS-OH30 NP with the same dosage were served as control group. At 1 h and 4 h incubation time points, cells were taken and followed by cell nuclei staining with Hoechst 33258 at 37°C.[25] Finally, the cells were imaged and analyzed by confocal laser scanning microscope (Leica TCS SP8, Wetzlar, DE, USA).[25]

In vivo wound healing assay

Ethics

All procedures, cares, and handling of the experimental animals were approved by the Ethics Committee of the Kunming Institute of Zoology at the Chinese Academy of Sciences or Weifang Medical University. Animal welfare was followed according to the eighth edition of the Guide for the Care and Use of Laboratory Animals (Institute for Laboratory Animal Research. 2011, Washington, DC: National Academies Press).

Macroscopic evaluation and measurement of the healing wound

KM mice were obtained from the Shanghai Animal Center (female, 6 weeks of age, and average weight: 20–25 g). The mice were first anesthetized under aseptic conditions. The dorsal skin was cleaned using hair clipper. A skin biopsy punch (ID = 7 mm) was placed perpendicular to the dorsal skin and pushed downward with a circular twisting motion. Then, the middle skin was removed. In this way, full-thickness excisional round wounds were created. The mice were randomly divided into four groups of saline control (untreated), the blank CMCS NP (CMCS), OH30 aqueous solution (OH30), and CMCS-OH30 NP. All experimental animals were given a single dosage every 24 h by using a sterile insulin syringe (BD, Franklin Lakes, NJ, USA). Wounds were administered with saline, blank CMCS NP, OH30, and CMCS-OH30 NP in a total volume of 100 μL. The final concentration of OH30 in both CMCS-OH30 NP and OH30 groups was 50 and 100 μg/mL CMCS NP was used in blank CMCS NP group. The mice in each group were separately placed in SPF animal house. During wound healing, each wound of the mice was observed, carefully recorded, and analyzed as described in the "Cell migration assay" section. The mice were then sacrificed on postoperative day 15.[29,30]

The nude mice (female, 6 weeks of age, and average weight: 20–25 g) were maintained in the Center for Experimental Animals (an AAALAC-accredited experimental animal facility) at Key Laboratory of Animal Models and Human Disease Mechanisms of the Chinese Academy of Sciences. When the wound was created, CMCS-OH30 NP (Cy5-labeled OH30) was administered on the dorsal skin as previously described, the dosages of CMCS-OH30 NP and OH30 used were the same as the administration for KM mice. The partial wound along with surrounding tissues was collected at 1 and 4 h. The OH30 distribution in the skin tissue was observed with a fluorescence microscope (Olympus, BX53F; Olympus Corporation). The mice were also monitored by near-infrared (NIR) fluorescence imaging (in vivo small animal imaging system, IVIS Lumina XR, Caliper Life Sciences, Hopkinton, MA, USA).[31]

Histopathological assessment

At the indicated time points, the collected wound and surrounding tissues after the injury were used for histological analysis. The samples (including an area of about 5 mm around the wound edge) were immediately fixed in 4% buffered formalin overnight. The wound tissue was embedded in paraffin blocks and sequentially sectioned at 5 μm. Finally, the skin sections were stained with H&E to evaluate the presence of necrosis inflammatory cells, hemorrhage, granulation tissue extent, re-epithelialization, and thick epidermis formation. Skin tissue was stained with a modified MT stain (Solarbio, Beijing, China) according to the manufacturer's protocol to explore the extent of collagen deposition and fibroblasts in healed tissue during wound healing.[32] Images were obtained with the microscope (Olympus, BX53F; Olympus Corporation).

Cytokines assay

As previously described, the wound tissues (100 mg) were rinsed with PBS, immersed in PBS, and homogenized by a high-speed tissue machine (IKA T10, Staufen, Germany) at 4°C for 5–10 min. Two freeze–thaw cycles were performed to break the cell membranes. The homogenates were added

with protease inhibitor and were centrifuged at 12,000 rpm and 4°C for 10 min. The supernatants were collected and stored at −80°C. Inflammatory cytokines (IL-6, IL-8, IL-10, TGF-β1, and TNF-α1) were quantified by the corresponding ELISA kits according to the protocols provided by the manufacturer (Proteintech, Chicago, IL, USA).

Collagen content in the healing skin assay

Collagen type I and type III contents were determined through the ELISA method according to the protocols provided by the producer. The supernatants prepared in the "Cytokines assay" section were used. Mouse collagen type I and type III detecting kits were purchased from Cusabio (Wuhan, China).

Statistical analysis

Data were collected and presented as the mean and the standard error of the mean. The experimental data in different groups were compared using one-way ANOVA in SPSS 15.0 software (SPSS Inc., Chicago, IL, USA). The values of $*p < 0.05$ and $**p < 0.01$ were considered statistically significant.

Results

Preparation, characterization, release, and stability studies of CMCS-OH30 NP

The peptide OH30 contains large amounts of lysine residues. Table 1 shows values of the particle size and zeta potential during the process of sequential alternate absorption of oppositely charged polyelectrolytes. CMCS-OH30 PNP is defined as the primary core of the final nanoparticle formed first through the alternate adsorption of oppositely charged CMCS and OH30. CMCS-OH30 PNP was recharged to the negative value of −36.7 (±3.3) mV. One CS layer was added to the CMCS-OH30 PNP shell to form CMCS-OH30 NP, and then the surface potential value was reversed to positive charged +30.2 (±5.1) mV, along with the mean particle size increased to 258.7 (±13.3) nm. The polydispersity index (PDI) value was less than 0.2. Accordingly to the ratio of initial materials (CS:CMCS:OH30 = 0.4:2:1), the final yield of the prepared nanoparticles was approximately 73%. The EE and LE were determined to be 82.46% (±1.11%) and 33.17% (±1.55%), respectively, which reflect the good loading capacity of NP. CMCS-OH30 NP showed little variation in size and zeta potential during the storage of 28 days at 4°C, suggested CMCS-OH30 NP had desirable stability (Figure S1).

TEM images revealed the process of OH30 release from nanoparticles. CMCS-OH30 NP was spherical with smooth surfaces when in the SWF solution (Figure 1A). After 4 h, the edges of the nanoparticles became irregular (Figure 1B). At 12 h, the debonding of the CS superficial layer gradually appeared due to the interaction untangling (Figure 1C). After 24 h, the shape of the nanoparticles was disintegrated (Figure 1D).

In vitro drug release and antimicrobial activity assay

To evaluate whether free OH30 was released from prepared nanoparticles and maintained biological activity, *E. coli* 25922 was randomly chosen to monitor the effects of CMCS-OH30 NP. As expected, CMCS-OH30 NP killed nearly 100% bacteria at each time intervals (Figure 2A). Comparatively, CMCS NP showed weaker antimicrobial activity and diminished after 12 h (Figure 2B).

In vitro internalization assay of CMCS-OH30 NP

Macrophages were one of the primary immune responding cell styles involving in wound healing.[33] RAW264.7 cells were used in cellular uptake assay to evaluate whether our prepared CMCS-OH30 NP enter the cells and exert its biological functions. Cy5-labeled OH30 and Hoechst 33258 stained nuclei emit red and blue fluorescence, respectively. Both the CMCS-OH30 NP and free OH30 all interacted with cell membranes due to their positive charges after 1 h incubation with the RAW264.7 cells. However, the uptake amount of OH30 in CMCS-OH30 NP-treated group was higher than that of free OH30-treated group (Figure 3A and C). Meanwhile, after 4 h incubation, the OH30 in

Table 1 Properties of CMCS-OH30 NP and CMCS NP (mean ± SD, n = 6)

Name	Mean particle size (nm)	PDI	Zeta potential (mV)	EE (%)	LE (%)
CMCS-OH30 PNP	198.3 ± 7.6	0.19 ± 0.07	−36.7 ± 3.3	89.33 ± 1.67	43.81 ± 1.79
CMCS-OH30 NP	258.7 ± 13.3	0.15 ± 0.03	+30.2 ± 5.1	82.46 ± 1.11	33.17 ± 1.55
Unloaded NP	133.2 ± 4.6	0.13 ± 0.04	−41.4 ± 1.6	NA	NA

Abbreviations: CMCS-OH30 NP, carboxymethyl chitosan nanoparticles; PDI, polydispersity index; EE, encapsulation efficiency; LE, loading efficiency.

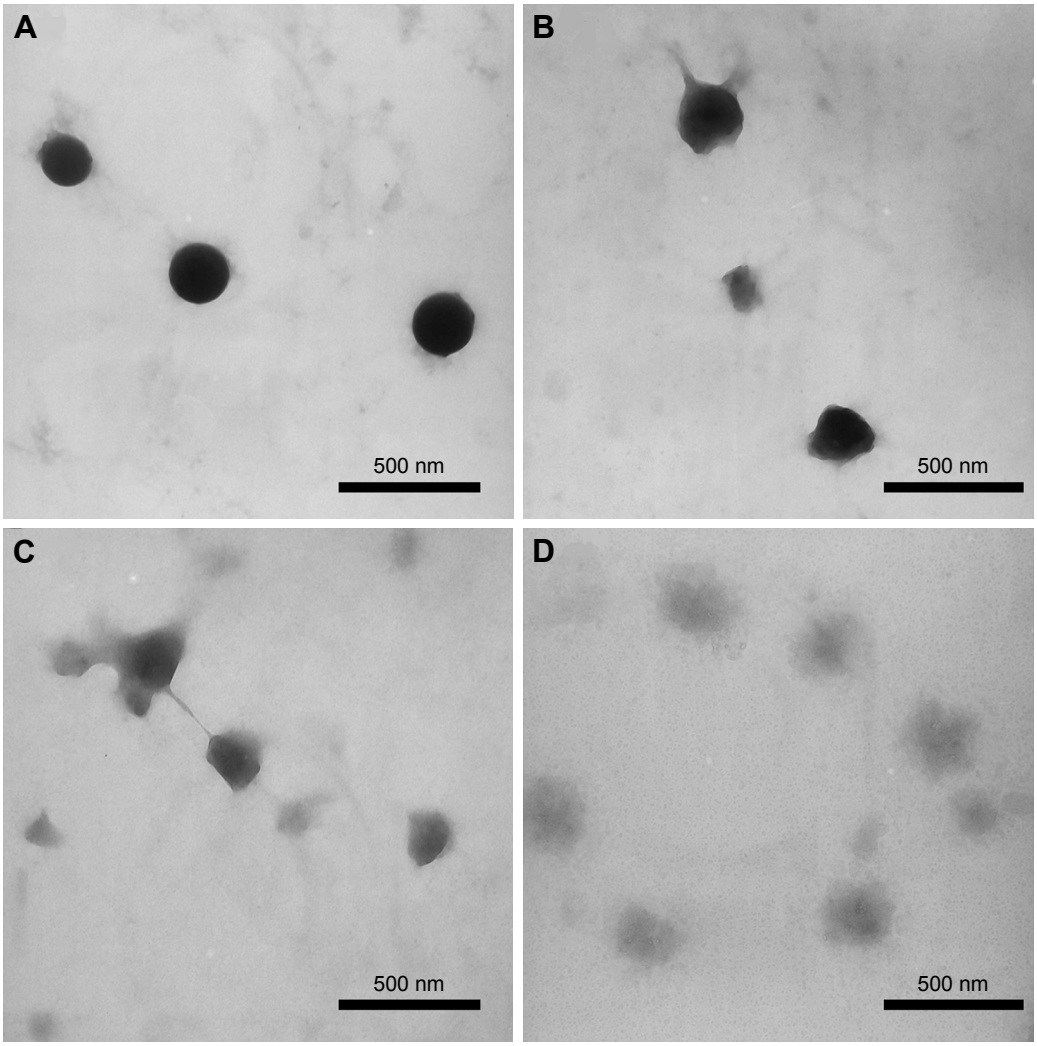

Figure 1 TEM images of CMCS-OH30 NP releasing in SWF solution (pH 7.4). (**A**) Initial shape in SWF, (**B**) 4 h in SWF, (**C**) 12 h in SWF, and (**D**) 24 h in SWF.
Abbreviations: CMCS-OH30 NP, carboxymethyl chitosan nanoparticles; SWF, simulated wound fluid.

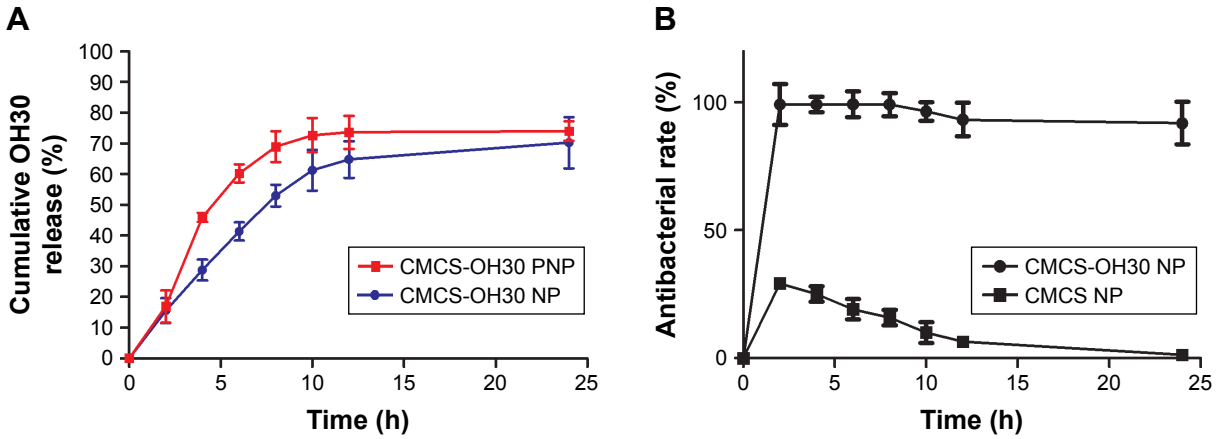

Figure 2 In vitro drug release curve and antimicrobial activity assay.
Notes: (**A**) In vitro release profile of OH30 (plotted as a function of % cumulative release vs time) from CMCS-OH30 NP (mean ± SD, n = 3). (**B**) Representative antibacterial activities of CMCS-OH30 NP and CMCS NP against the *E. coli* (mean ± SD, n = 3). Three independent experiments were carried out and each tested points was triplicated in all experiments.
Abbreviations: CMCS-OH30 NP, carboxymethyl chitosan nanoparticles; *E. coli*, *Escherichia coli*.

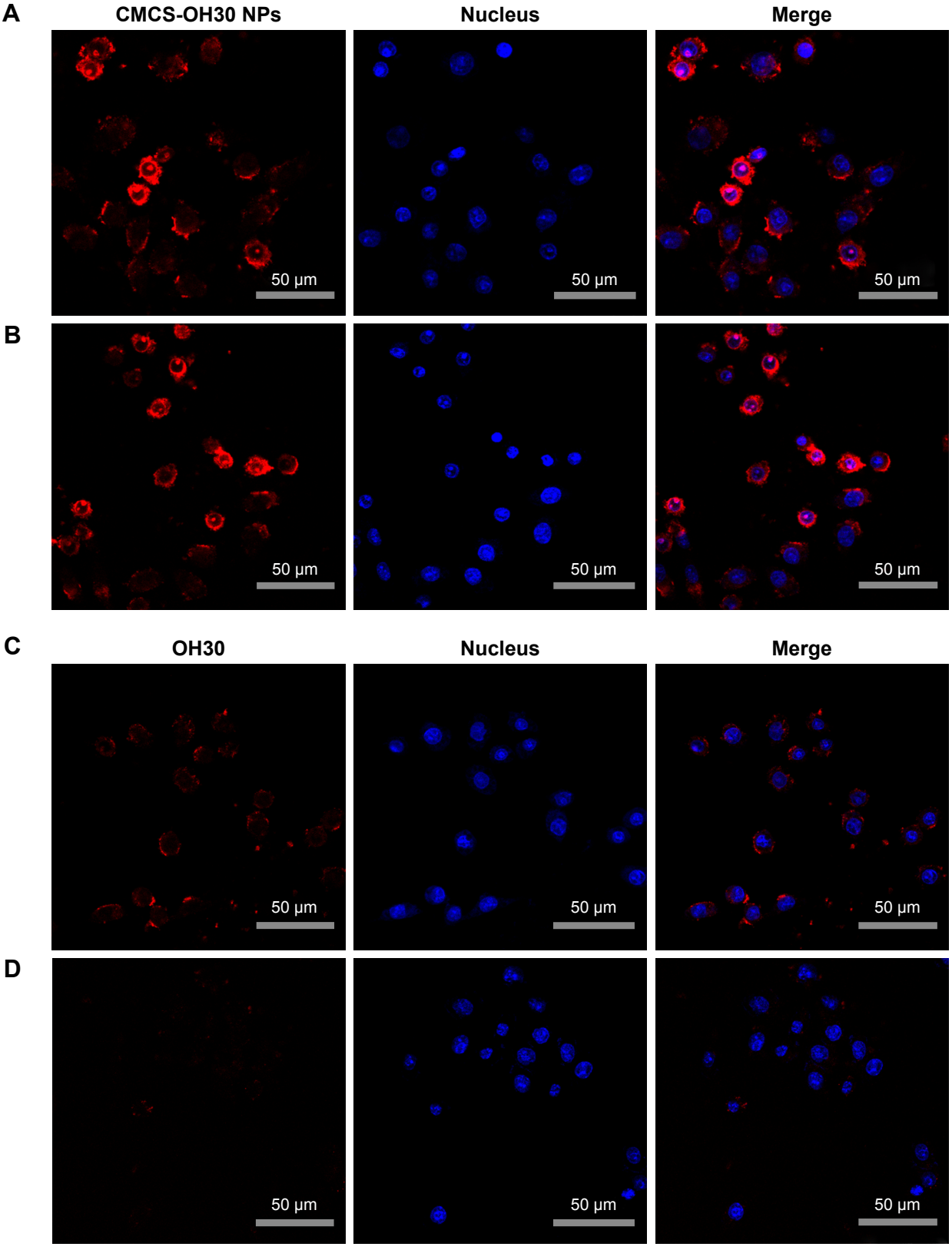

Figure 3 Internalization of OH30 in RAW264.7 cells were detected by confocal laser scanning microscope.
Notes: Cells were treated with CMCS-OH30 NP at 37°C for 1 h (**A**) and 4 h (**B**). Cells were treated with free OH30 at 37°C for 1 h (**C**) and 4 h (**D**). Nuclei were stained with Hoechst 33258 (blue) and OH30 labeled by Cy5 (red).
Abbreviation: CMCS-OH30 NP, carboxymethyl chitosan nanoparticles.

macrophages became more concentrated and entered into the cytoplasm in the CMCS-OH30 NP group compared with free OH30-treated group (Figure 3B and D). It should be noted that after 4 h incubation, red fluorescence signal from free OH30 group almost disappeared (Figure 3D). Two possible reasons might be responsible for these phenomena: first, digested OH30 could not bind and are untaken by the cells; second, CMCS not only stabilizes the OH30 but also releases free OH30 in a controlled manner and might help in the binding of released OH30 interaction with membrane, thus promoting the internalization of the OH30 in macrophages.

In vitro cell migration and proliferation

Keratinocytes play a pivotal role in wound closure in the later inflammation and proliferation phases. A modified scratch assay was conducted to determine the migration and proliferation abilities of CMCS-OH30 NP, CMCS, and OH30. Compared with the untreated control group, 50 μg/mL of CMCS NP, OH30, and CMCS-OH30 NP experimental groups all showed better migration effects on human keratinocyte HaCaT cells (Figure 4). Statistically, CMCS-OH30 NP group showed a better cell migration rate than both CMCS NP and OH30 within 12 and 24 h. The cytotoxicity of OH30, CMCS NP, and CMCS-OH30 NP on HaCaT and

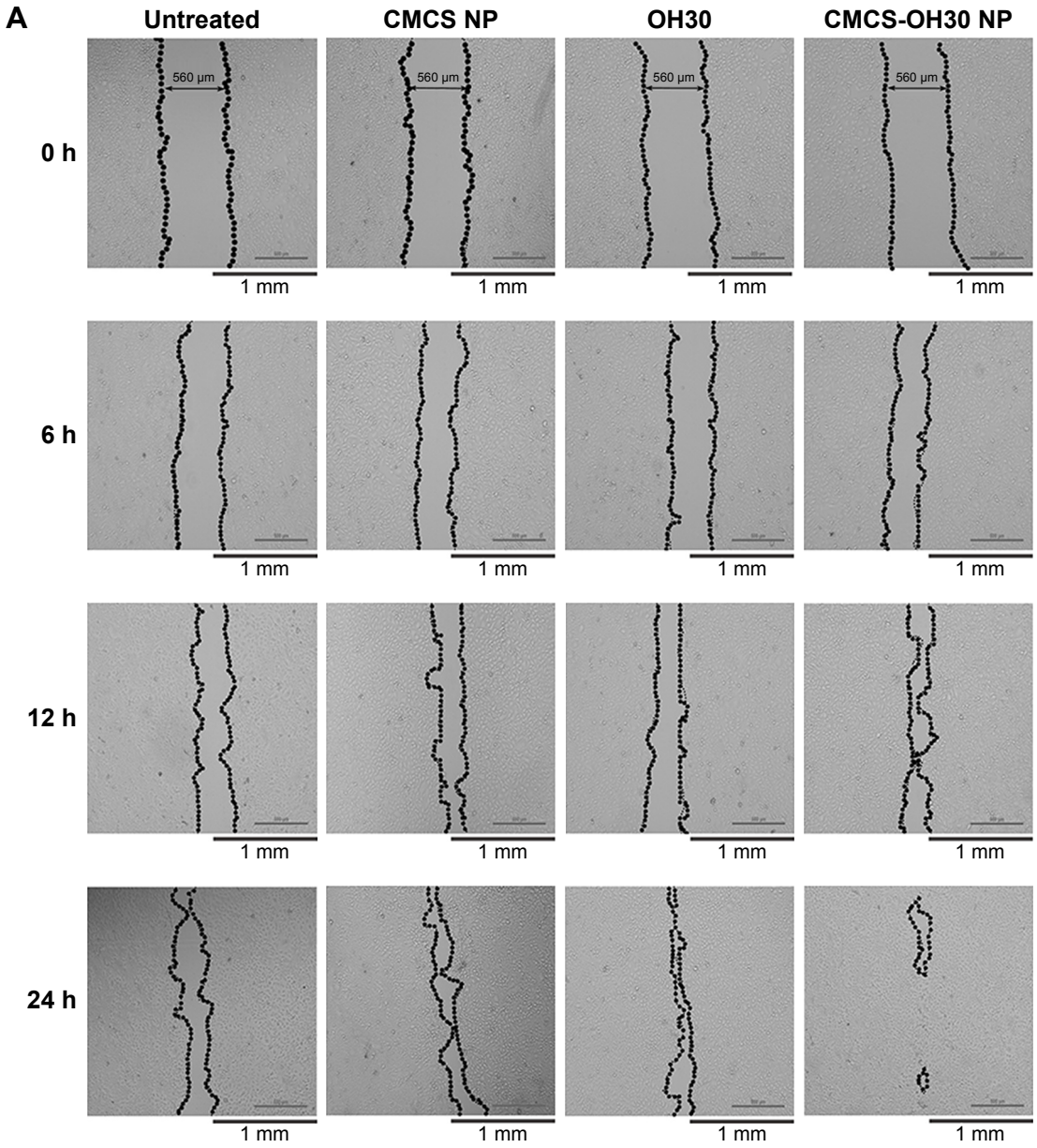

Figure 4 (*Continued*)

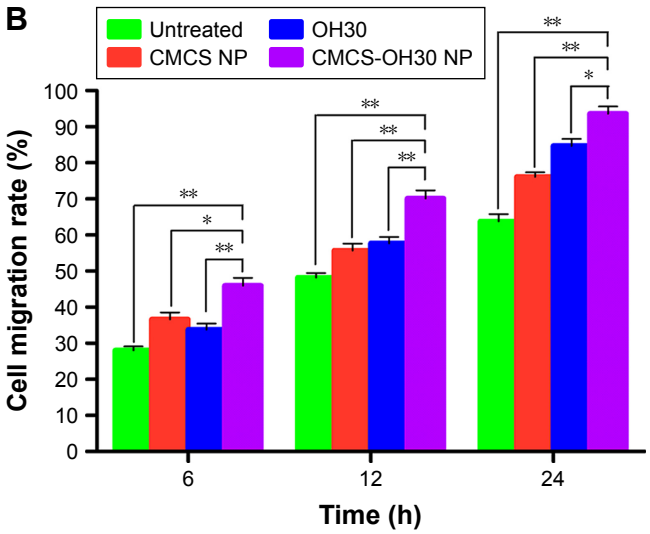

Figure 4 In vitro HaCaT cell migration assays.
Notes: (**A**) Effects of untreated, CMCS NP, OH30, and CMCS-OH30 NP were assessed by microscope images. (**B**) Cell migration rates of each group were expressed as percentage of initial blank area. Statistical significance compared with other groups (mean ± SD; n = 4; *$p < 0.05$ and **$p < 0.01$).
Abbreviation: CMCS-OH30 NP, carboxymethyl chitosan nanoparticles.

BJ fibroblast cells was also investigated. No cytotoxicity was detected during the 48 h incubation of OH30 (0–100 μg/mL) with HaCaT, BJ fibroblast, and RAW264.7 cells.

In vivo wound healing assays

In vivo wound skin adhesion and permeation

To avoid animal skin noise by fluorescence microscopy and in vivo small animal imaging system IVIS Lumina XR, a living nude mouse model with full-thickness wound was established to verify the wound-adhesive capacity and drug delivery of the prepared nanoparticles. With the 24 h treatment, the fluorescence intensity of the wound area gradually weakened (Figure S2). To verify whether labeled OH30 was delivered into the subcutaneous tissues, the distribution of labeled OH30 in the skin tissues at OH30-loaded NP and free OH30 groups after 1 and 4 h posttreatment was investigated by fluorescence microscopy (Figure 5). Comparison with the free OH30 group, the distribution of labeled-OH30 in the skin tissues of OH30-loaded NP group was quite similar (Figure 5A and C). However, after 4 h treatment, the fluorescence signals of OH30-loaded NP group existed all over the tissue and appeared at the bottom of the picture, which indicated that Cy5-OH30 was delivered into the subcutaneous tissues (Figure 5B). Meanwhile, the fluorescence signals of free OH30 group were hard to detect and reflecting the active peptide might be digested by enzymes. Taken together, these images suggested that CMCS-OH30 NP could be protected from early degradation, release in controlled manner, and permeate into deeper skin layers in animal models.

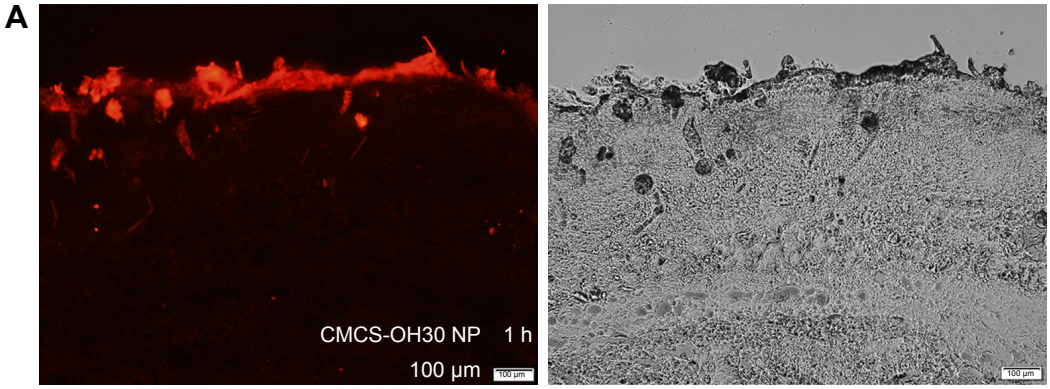

Figure 5 (*Continued*)

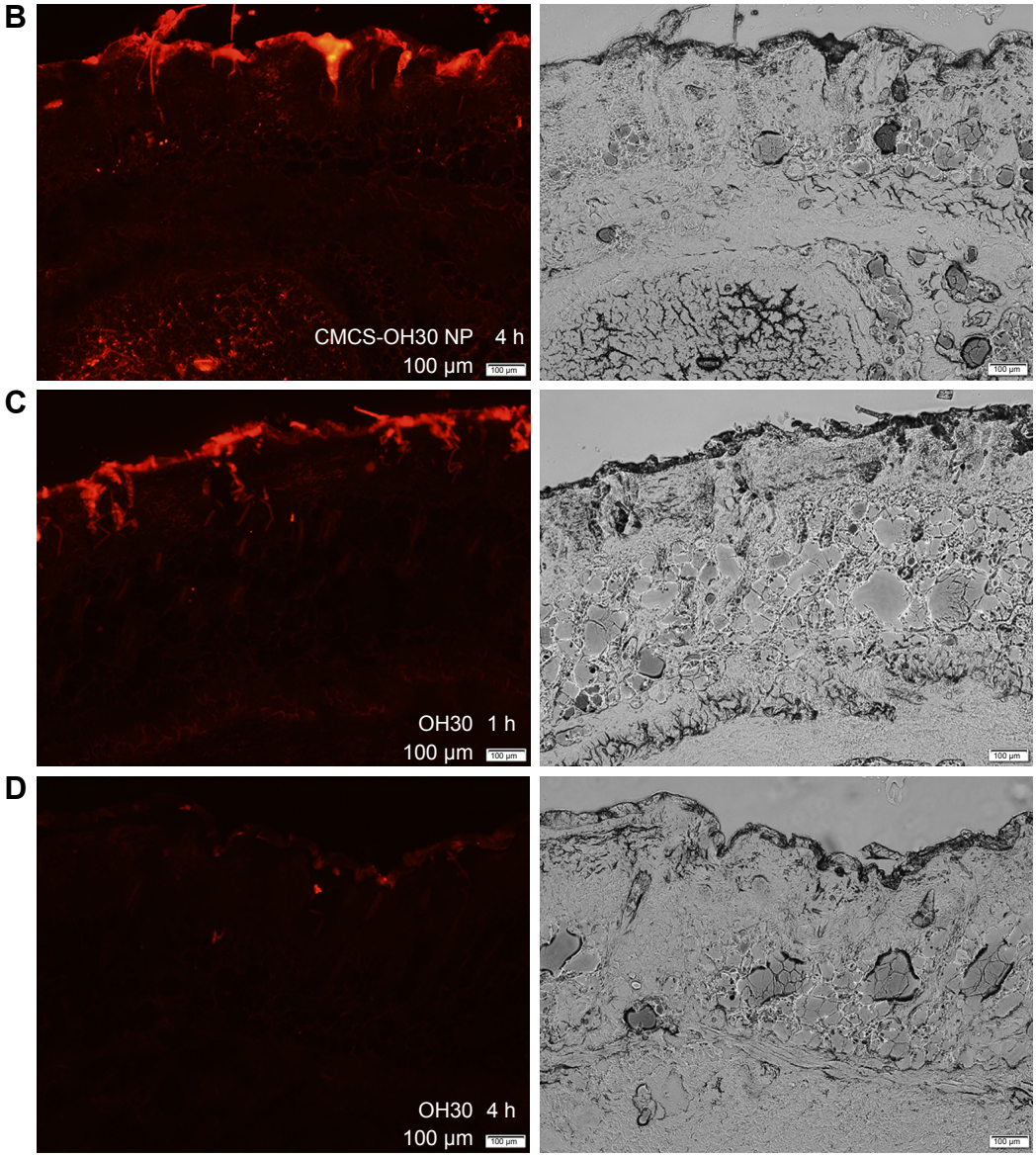

Figure 5 Distribution of CMCS-OH30 NP in the nude mouse skin tissue observed by fluorescence microscope.
Notes: Images of CMCS-OH30 NP at 1 h (**A**) and 4 h (**B**) posttreatment; images of free OH30 at 1 h (**C**) and 4 h (**D**) posttreatment. OH30 used was labeled with Cy5 (red).
Abbreviation: CMCS-OH30 NP, carboxymethyl chitosan nanoparticles.

In vivo wound healing effects

Macroscopic observations of wound closure at the day 0, 5, 10, and 15 postinjury are shown in Figure 6. In general, CMCS-OH30 NP group significantly accelerated wound closure and benefit nonscar healing at all tested points compared with other groups (Figure 6A). Five days after the operation, CMCS-OH30 NP group showed a faster wound closure rate of 69.33% (±2.41%), whereas the other groups maintained a wound closure rate in the range of 36.12%–58.31% (Figure 6B). As expected, the constructed nanosystem has a significant role in early stage of wound healing. On the 15th postoperative day, free OH30- and CMCS-OH30 NP-treated groups displayed much smaller, smooth, and with lighter color, compared with rest groups, especially for topical administration of CMCS-OH30 NP, no obvious scar existed (Figure 6A). Free OH30 showed better effects than that of nanocarrier at all tested points. Both of them showed a good potential to enhance the wound healing when compared with negative untreated group.

The microscopic investigation of the healing wounds skin sections at day 15 postinjury in four tested groups by MT staining and H&E staining revealed that the quality of wound recovery is different (Figure 7). The wound skin treated with CMCS-OH30 NP formed a clear, smooth, and intense re-epithelialization layer. In comparison, incomplete re-epithelialization and multiple invaginated

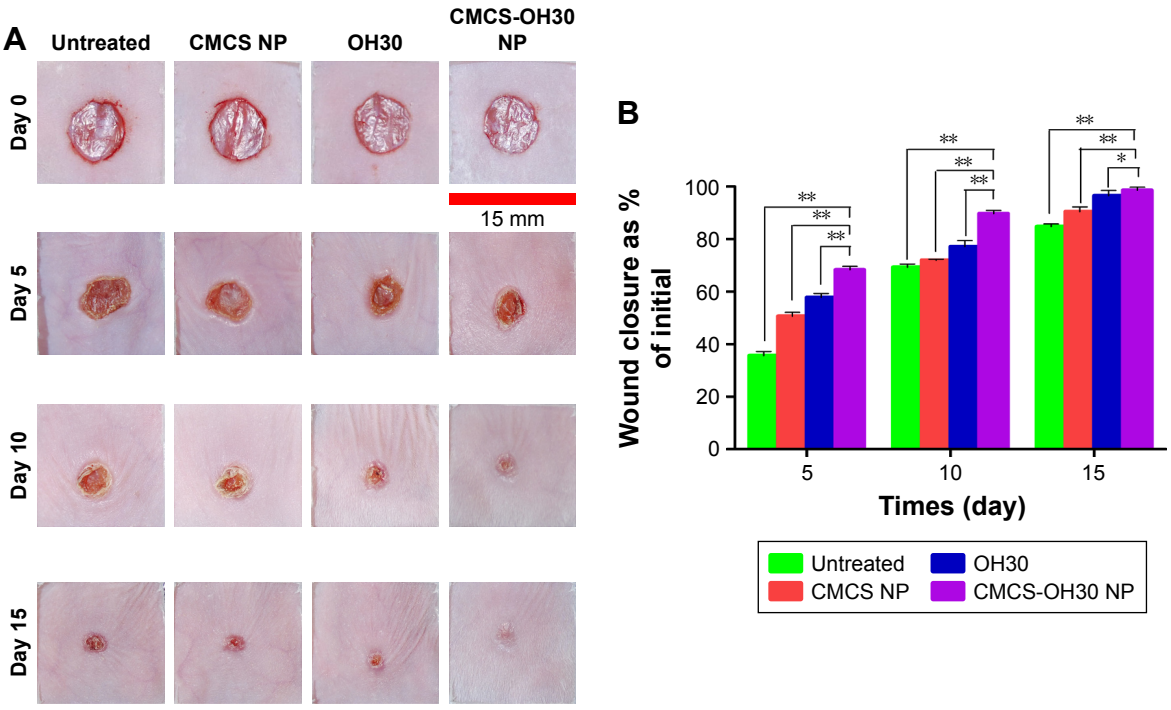

Figure 6 Wound healing effects on mice models.
Notes: (**A**) Macroscopic observations of wound closure for different treated groups at day 0, 5, 10, and 15 postinjury. The initial wounds were round (ID = 7 mm). (**B**) Wound closure rate of all groups. Data were presented as mean ± SD, n = 6. *$p < 0.05$ and **$p < 0.01$, contrast with other groups.
Abbreviation: CMCS-OH30 NP, carboxymethyl chitosan nanoparticles.

epidermises (the area pointed out by the green arrow) were observed in the contrast groups (Figure 7A and B). The newly formed skin in OH30 and CMCS-OH30 NP groups underwent re-epithelialization with a clear smooth thick epidermis and had well-defined hair follicle structures at day 15 postinjury; these findings are considered as positive signs. Meanwhile, in rest of the experimental groups, the boundary was unclear and irregular between the epidermis and the dermis, which generated multiple invasions and adhesions and thus led to macroscopic irregularity and scar formation.

In vivo evaluation of the status of collagen I and III after treatment

Collagen deposition/maturation shows sustained effects on scar formation, especially collagen I and III. To investigate

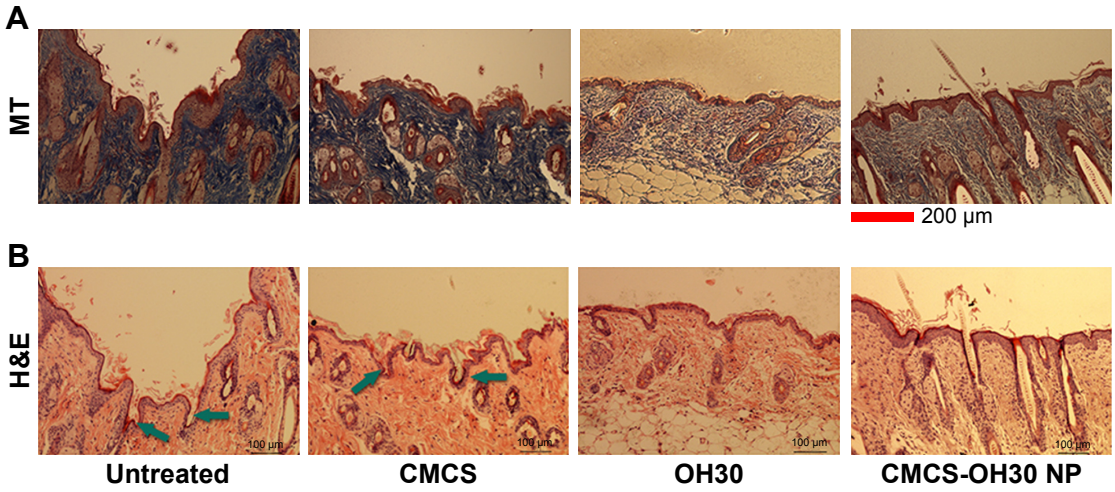

Figure 7 Histological examination of the healing wounds skin sections at day 15 postinjury in four tested groups.
Notes: MT staining (**A**) and H&E staining (**B**). The green arrow indicated the multiple invaginated epidermises. Scale bars = 200 μm.
Abbreviations: CMCS-OH30 NP, carboxymethyl chitosan nanoparticles; MT, Masson's trichrome; H&E, hematoxylin and eosin.

the mechanism of CMCS-OH30 NP reducing skin scar formation, we quantified the concentrations of both collagen I and collagen III in skin tissues at day 15. Interestingly, collagen I showed the lowest content in skin homogenate of CMCS-OH30 NP group 15 days after injury among all the tested groups (Figure 8A), whereas the collagen III content in CMCS-OH30 NP group showed the highest (Figure 8B). Thus, the ration of collagen I and collagen III in CMCS-OH30 NP group appeared to be the lowest among the tested groups (Figure 8C). However, CMCS-OH30 NP showed a statistical significance in reducing the concentration of collagen I in the newly grown tissues from 220 ng/μg in untreated group to 60 ng/μg in CMCS-OH30 NP, but the content of collagen III only increased from 18 to 32 ng/μg in both groups, respectively. These resulted in the total content of collagen I plus collagen III in CMCS-OH30 NP group also lowest in all the experimental groups (Figure 8D). CMCS-OH30 NP treatment prevented the excess collagen accumulation to form scar.

Regulation of cytokines during wound healing in vivo

Many factors, especially cytokines, are attributed to wound healing. Thus, the concentrations of IL-6, IL-8, IL-10, TGF-β1, and TNF-α1 were quantified in the skin lysates of the experimental animals. The proinflammatory cytokines IL-6 and IL-8 had higher concentrations in CMCS-OH30 NP group 3 days after the treatments. However, both of these cytokines showed a steady decrease compared with the saline group at days 5 and 10 (Figure 9A and B). The effect on another proinflammatory cytokine, TNF-α1, was different. CMCS-OH30 NP reduced TNF-α1 at day 3 compared with the saline group; however, OH30 exhibited an increasing effect compared with the untreated group. This phenomenon might be caused by the tendency of CMCS to suppress TNF-α1 expression. At days 5 and 10, CMCS-OH30 NP showed inhibitory effect on TNF-α1 expression (Figure 9E). Interestingly, CMCS-OH30 NP significantly boosted the anti-inflammation cytokine IL-10 expression at both days 3 and 5. The IL-10 concentration remained

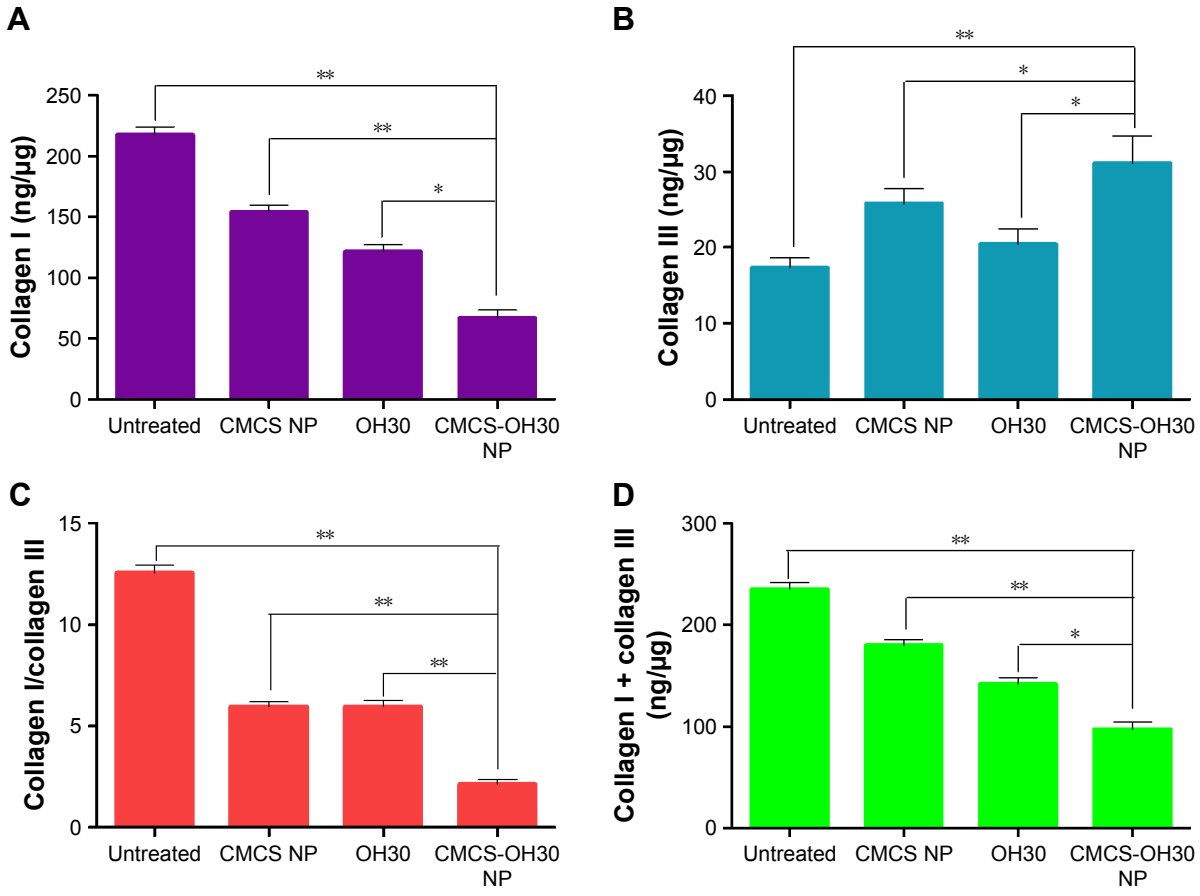

Figure 8 Quantification of collagen I and III content in skin homogenate 15 days after injury.
Notes: The content of collagen I (**A**), the content of collagen III (**B**), the ratio of collagen I and collagen III (**C**), and the total content of collagen I plus collagen III (**D**). Statistical significance of CMCS-OH30 NP group was compared with other groups (mean ± SD; n = 6, Student's *t*-test. $*p < 0.05$ and $**p < 0.01$).
Abbreviation: CMCS-OH30 NP, carboxymethyl chitosan nanoparticles.

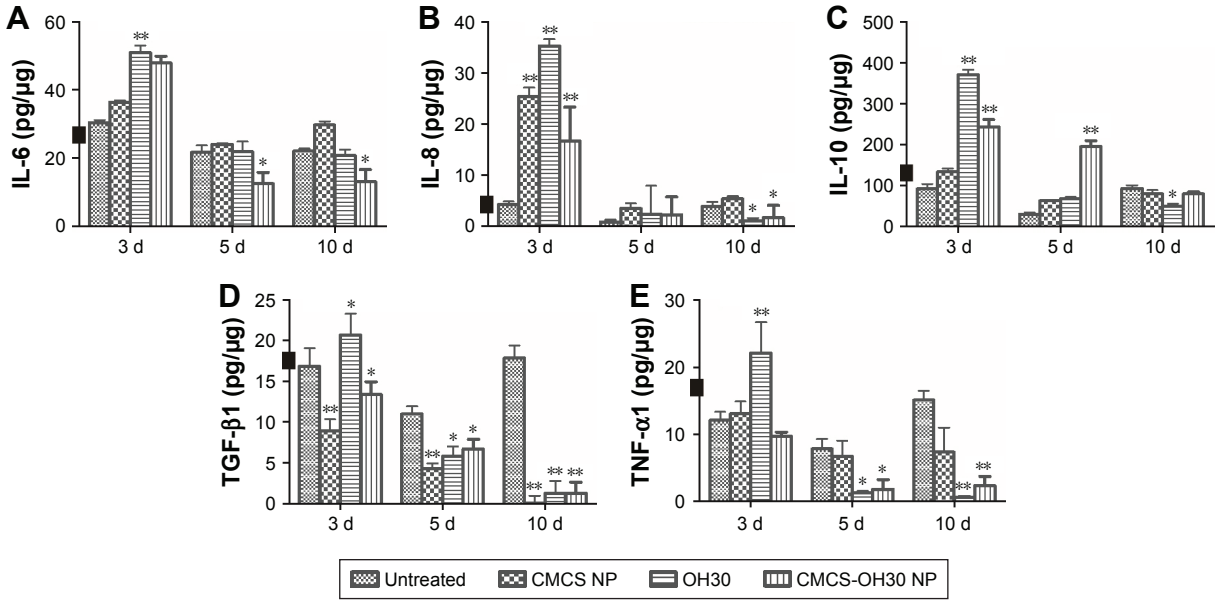

Figure 9 Quantification of cytokines in skin lysates.
Notes: IL-6 (**A**), IL-8 (**B**), IL-10 (**C**), TGF-β1 (**D**), and TNF-α1 (**E**). The black boxes ■ on the *y*-axis refer to the quantification level of cytokines in normal mouse skin. Statistical significance compared with the untreated group was indicated (mean ± SD; n = 6, Student's *t*-test. *$p < 0.05$ and **$p < 0.01$).
Abbreviations: CMCS-OH30 NP, carboxymethyl chitosan nanoparticles; d, days.

normal at day 10 (Figure 9C). CMCS-OH30 NP exhibited an inhibitory effect on the expression of TGF-β1 at all tested time intervals (Figure 9D).

Discussion

Nanotechnology provides a novel method to overcome the disadvantage of using peptide-based agents, especially in controlling the release and avoiding the digestion by enzymes.[34,35] In recent years, material-based drug delivery systems have been used to expand applications of bioactive proteins and peptides, especially in wound healing applications.[36–38] Cytokine FGFs were incorporated into composite CMCS hydrogel for accelerating skin regeneration by enhancing skin permeability and avoiding rapid degradation.[18] CMCS-encapsulated insulin showed better outcomes in epithelial permeation, bioavailability, and half-time than single insulin application.[21] Human LL-37 is a well-documented molecule that belongs to the cathelicidin family and has important roles in innate immunity.[33] Topical treatment with LL-37 for chronic leg ulcers in humans revealed that LL-37 has a significant effect on hard-to-heal wound healing.[9] LL37 encapsulated in PLGA nanoparticles (PLGA-LL37 NP) successfully avoids the immediate degradation and inactivation of LL37. However, methylene dichloride as an organic solvent in the preparation of PLGA-LL37 NP exhibits negative effects in the wound environment.[24]

In the present investigation, we successfully encapsulated OH30 within CMCS and CS through the ionic gelation method under mild conditions. The prepared CMCS-OH30 NP showed good slow releasing properties both in vitro and in vivo. The average release rate of OH30 liberated from CMCS-OH30 NP was 6.53 ± 1.13 μg/mL·h in the initial 10 h and free OH30 could continuously release for at least 24 h. Attributing to the double layer and internal structure, CMCS-OH30 NP group showed a near-liner cumulative release profile of OH30 at the early 12 h. Its average release rate was 6.53 (±1.13) μg/mL·h, much slower than CMCS-OH30 PNP. The final cumulative release amount reached to 70.25 (±8.40)% at 24 h was detected. The release mechanism of the prepared CMCS-OH30 NP might be caused by 1) positively charged OH30 binding sites are filled and replaced with sodium ions or other ions contained in the environment, which loosen the linkage of OH30 with nanocarriers; and/or 2) the existed strong electrolytes also affected the interactions of CMCS and CS, making the interaction weak and collapsing of the NP structure. Therefore, the release of OH30 from the CMCS NP might be attributed to the combination of the absorption weakening, construct collapsing in the electrolyte solution, and OH30 diffusion.

Our previous work demonstrated that OH30 showed a broad antibacterial spectrum against various bacterial.[12–15] Moreover, it was reported that OH30 lost approximately 80% antibacterial activity against *E. coli* 25922 after incubation

with 100% human serum for 3 h.[14] In vitro drug release and antimicrobial activity assays demonstrated the OH30 released form NP remained its biological activity and could be active for at least 24 h by controlled release from prepared nanoparticles. Consistent with our previous results, present in vitro cellular uptaken assay and in vivo skin tissue distribution experiments indicated that free OH30 could not last 4 h in enzymatic fluid. However, the prepared NP acquired the ability to continuously release free OH30 and help to maintain its activity both inside the cells and in deeper skin area (Figures 3 and 5). In full-thickness wound models, the prepared NP showed significantly fast wound healing and nonscarring results in all the tested groups (Figure 6). The quality of the healing wound in the prepared NP also showed best signals among the tested groups as revealed by MT and H&E staining, as well as the content and ratio of collagen I and III (Figures 7 and 8).

Human LL37 and OH30 showed varied immune regulation activities, although both molecules belong to the same cathelicidin AMP family.[14,16] The immune regulation activity of OH30 is partly attributed to its CCL2 and CXCL2 chemokine-inducing activities. OH30 also selectively regulates cytokine expression. The levels of anti-inflammatory cytokines of IL-10 and IL-1Ra were largely increased both at the mRNA and at the protein levels, whereas the proinflammatory cytokines of TNF-α, IL-1β, and IL-6 showed no significant changes in the mouse peritoneal lavage, 5 h after an intraperitoneal injection of OH30.[16]

Consistent with our previous results, the present in vivo experiments revealed that the concentration of proinflammatory cytokine of IL-6 slightly increased after the topical treatment of CMCS-OH30 NP for 3 days but significantly decreased after 5 and 10 days. Other proinflammatory cytokines of IL-8, TGF-1, and TNF-1 showed obvious decrease in all tested points at the protein levels. The anti-inflammatory cytokine IL-10 concentration significantly increased for 5 days compared with that in the saline control. The upregulation of IL-10 inhibits the inflammatory response and minimizes the abnormal collagen and extracellular matrix compositions to favor the scarless wound healing.[40,41] Although CMCS NP and OH30 exhibited slight differences in inducing the expression of pro- and anti-inflammatory cytokines, the prepared CMCS-OH30 NP showed better immunoregulatory effect on the scar-free wound healing. For example, CMCS NP showed the best reducing effects on TGF-1 expression compared with OH-30 and CMCS-OH30 NP at all tested points. However, the TGF-1 concentration was reduced by CMCS-OH30 NP but increased by the native agent 3 days after the treatment compared with the saline control. Meanwhile, at the late stage of wound healing, the ratio and content of collage I and III also showed a good tendency favorite nonscaring healing. Taken together, CMCS-OH30 NP inherited the advantages of both CMCS NP and OH30. By rebalancing the immunoresponse of the wound, an anti-inflammatory microenvironment around the wound is created to facilitate nonscarring wound healing.

Conclusion

A novel CMCS-OH30 NP was prepared through ionic gelation method under mild conditions. The prepared nanoparticles possessed the advantages of both OH30 and CMCS and can release free OH30 for 24 h. The released OH30 is beneficial to nonscarring wound healing via downregulation of immune responses at the early steps in wound healing which in turn has an important role to affect both collagen I and III at the late stage in wound healing process. A better result was observed in the full-thickness wound animal model. The use of nanotechnology to encapsulate immune regulation molecules might be a good solution for wound healing treatment.

Acknowledgments

This work was supported by National Natural Science Foundation of China (NSFC: 81673576, 31600775, and 81373945), Shandong Provincial Natural Science Foundation, China (ZR2015HL056, ZR2015HL061, and ZR2016HM76), A Project of Shandong Province Higher Educational Science and Technology Program (J15LM10), A Project of Shandong Province Medical and Health Technology Development Program (2015WS0059), and the Public School Teachers Domestic Visits Program of Weifang Medical University.

Disclosure

The authors report no conflicts of interest in this work.

References

1. Eming SA, Martin P, Tomic-Canic M. Wound repair and regeneration: mechanisms, signaling, and translation. *Sci Transl Med*. 2014; 6(265):265sr6.
2. Martin P, Nunan R. Cellular and molecular mechanisms of repair in acute and chronic wound healing. *Br J Dermatol*. 2015;173(2):370–378.
3. Dzialo M, Mierziak J, Korzun U, Preisner M, Szopa J, Kulma A. The potential of plant phenolics in prevention and therapy of skin disorders. *Int J Mol Sci*. 2016;17(2):160.
4. Pereira RF, Barrias CC, Granja PL, Bartolo PJ. Advanced biofabrication strategies for skin regeneration and repair. *Nanomedicine (Lond)*. 2013;8(4):603–621.
5. Orlowski P, Zmigrodzka M, Tomaszewska E, et al. Tannic acid-modified silver nanoparticles for wound healing: the importance of size. *Int J Nanomedicine*. 2018;13:991–1007.

6. Behm B, Babilas P, Landthaler M, Schreml S. Cytokines, chemokines and growth factors in wound healing. *J Eur Acad Dermatol Venereol*. 2012;26(7):812–820.
7. Zhang Y. Why do we study animal toxins? *Zool Res*. 2015;36(4):183–222.
8. Mahlapuu M, Hakansson J, Ringstad L, Bjorn C. Antimicrobial peptides: an emerging category of therapeutic agents. *Front Cell Infect Microbiol*. 2016;6:194.
9. Gronberg A, Mahlapuu M, Stahle M, Whately-Smith C, Rollman O. Treatment with LL-37 is safe and effective in enhancing healing of hard-to-heal venous leg ulcers: a randomized, placebo-controlled clinical trial. *Wound Repair Regen*. 2014;22(5):613–621.
10. Wiig ME, Dahlin LB, Friden J, et al. PXL01 in sodium hyaluronate for improvement of hand recovery after flexor tendon repair surgery: randomized controlled trial. *PLoS One*. 2014;9(10):e110735.
11. Edsfeldt S, Holm B, Mahlapuu M, Reno C, Hart DA, Wiig M. PXL01 in sodium hyaluronate results in increased PRG4 expression: a potential mechanism for anti-adhesion. *Ups J Med Sci*. 2016;122(1):28–34.
12. Zhao H, Gan TX, Liu XD, et al. Identification and characterization of novel reptile cathelicidins from elapid snakes. *Peptides*. 2008;29(10):1685–1691.
13. Zhang Y, Zhao H, Yu GY, et al. Structure-function relationship of king cobra cathelicidin. *Peptides*. 2010;31(8):1488–1493.
14. Li SA, Lee WH, Zhang Y. Efficacy of OH-CATH30 and its analogs against drug-resistant bacteria in vitro and in mouse models. *Antimicrob Agents Chemother*. 2012;56(6):3309–3317.
15. Li SA, Liu J, Xiang Y, Wang YJ, Lee WH, Zhang Y. Therapeutic potential of the antimicrobial peptide OH-CATH30 for antibiotic-resistant *Pseudomonas aeruginosa* keratitis. *Antimicrob Agents Chemother*. 2014;58(6):3144–3150.
16. Li SA, Xiang Y, Wang YJ, Liu J, Lee WH, Zhang Y. Naturally occurring antimicrobial peptide OH-CATH30 selectively regulates the innate immune response to protect against sepsis. *J Med Chem*. 2013;56(22):9136–9145.
17. Samy RP, Sethi G, Lim LH. A brief update on potential molecular mechanisms underlying antimicrobial and wound-healing potency of snake venom molecules. *Biochem Pharmacol*. 2016;115:1–9.
18. Liu Q, Huang Y, Lan Y, et al. Acceleration of skin regeneration in full-thickness burns by incorporation of bFGF-loaded alginate microspheres into a CMCS-PVA hydrogel. *J Tissue Eng Regen Med*. 2017;11(5):1562–1573.
19. Wang G, Lu G, Ao Q, Gong Y, Zhang X. Preparation of cross-linked carboxymethyl chitosan for repairing sciatic nerve injury in rats. *Biotechnol Lett*. 2010;32(1):59–66.
20. Wang J, Xu M, Cheng X, et al. Positive/negative surface charge of chitosan based nanogels and its potential influence on oral insulin delivery. *Carbohydr Polym*. 2016;136:867–874.
21. Tsai WH, Yu KH, Huang YC, Li CI. EGFR-targeted photodynamic therapy by curcumin-encapsulated chitosan/TPP nanoparticles. *Int J Nanomedicine*. 2018;13:903–916.
22. Chen X, Park H. Chemical characteristics of O-carboxymethyl chitosans related to the preparation conditions. *Carbohydr Polym*. 2003;53(4):355–359.
23. Li X, Fan R, Tong A, et al. In situ gel-forming AP-57 peptide delivery system for cutaneous wound healing. *Int J Pharm*. 2015;495(1):560–571.
24. Chereddy KK, Her CH, Comune M, et al. PLGA nanoparticles loaded with host defense peptide LL37 promote wound healing. *J Control Release*. 2014;194:138–147.
25. Gao Y, Cheng X, Wang Z, et al. Transdermal delivery of 10,11-methylenedioxycamptothecin by hyaluronic acid based nanoemulsion for inhibition of keloid fibroblast. *Carbohydr Polym*. 2014;112:376–386.
26. Dongargaonkar AA, Bowlin GL, Yang H. Electrospun blends of gelatin and gelatin-dendrimer conjugates as a wound-dressing and drug-delivery platform. *Biomacromolecules*. 2013;14(11):4038–4045.
27. Casciaro B, Moros M, Rivera-Fernandez S, Bellelli A, de la Fuente JM, Mangoni ML. Gold-nanoparticles coated with the antimicrobial peptide esculentin-1a(1-21)NH2 as a reliable strategy for antipseudomonal drugs. *Acta Biomater*. 2017;47:170–181.
28. Di Grazia A, Cappiello F, Imanishi A, et al. The frog skin-derived antimicrobial peptide esculentin-1a(1-21)NH2 promotes the migration of human HaCaT keratinocytes in an EGF receptor-dependent manner: a novel promoter of human skin wound healing? *PLoS One*. 2015;10(6):e0128663.
29. Steinstraesser L, Lam MC, Jacobsen F, et al. Skin electroporation of a plasmid encoding hCAP-18/LL-37 host defense peptide promotes wound healing. *Mol Ther*. 2014;22(4):734–742.
30. Mei D, Lin Z, Fu J, et al. The use of alpha-conotoxin ImI to actualize the targeted delivery of paclitaxel micelles to alpha 7 nAChR-overexpressing breast cancer. *Biomaterials*. 2015;42:52–65.
31. Guo S, Huang Y, Zhang W, et al. Ternary complexes of amphiphilic polycaprolactone-graft-poly (N,N-dimethylaminoethyl methacrylate), DNA and polyglutamic acid-graft-poly(ethylene glycol) for gene delivery. *Biomaterials*. 2011;32(18):4283–4292.
32. Hardwicke JT, Hart J, Bell A, Duncan R, Thomas DW, Moseley R. The effect of dextrin-rhEGF on the healing of full-thickness, excisional wounds in the (db/db) diabetic mouse. *J Control Release*. 2011;152(3):411–417.
33. Zhang LJ, Sen GL, Ward NL, et al. Antimicrobial peptide LL37 and MAVS signaling drive interferon-beta production by epidermal keratinocytes during skin injury. *Immunity*. 2016;45(1):119–130.
34. Bhavsar S, Mudaliar S, Cherrington A. Evolution of exenatide as a diabetes therapeutic. *Curr Diabetes Rev*. 2013;9(2):33.
35. Sun BK, Siprashvili Z, Khavari PA. Advances in skin grafting and treatment of cutaneous wounds. *Science*. 2014;346(6212):941–945.
36. Zhao L, Chen D, Yao Q, Li M. Studies on the use of recombinant spider silk protein/polyvinyl alcohol electrospinning membrane as wound dressing. *Int J Nanomedicine*. 2017;12:8103–8114.
37. Li X, Ye X, Qi J, et al. EGF and curcumin co-encapsulated nanoparticle/hydrogel system as potent skin regeneration agent. *Int J Nanomedicine*. 2016;11:3993–4009.
38. Li Z, Liu M, Wang H, Du S. Increased cutaneous wound healing effect of biodegradable liposomes containing madecassoside: preparation optimization, in vitro dermal permeation, and in vivo bioevaluation. *Int J Nanomedicine*. 2016;11:2995–3007.
39. Asati A, Santra S, Kaittanis C, Perez JM. Surface-charge-dependent cell localization and cytotoxicity of cerium oxide nanoparticles. *ACS Nano*. 2010;4(9):5321–5331.
40. Peranteau WH, Zhang L, Muvarak N, et al. IL-10 overexpression decreases inflammatory mediators and promotes regenerative healing in an adult model of scar formation. *J Invest Dermatol*. 2008;128(7):1852–1860.
41. Coorens M, Scheenstra MR, Veldhuizen EJ, Haagsman HP. Interspecies cathelicidin comparison reveals divergence in antimicrobial activity, TLR modulation, chemokine induction and regulation of phagocytosis. *Sci Rep*. 2017;7:40874.

Supplementary materials

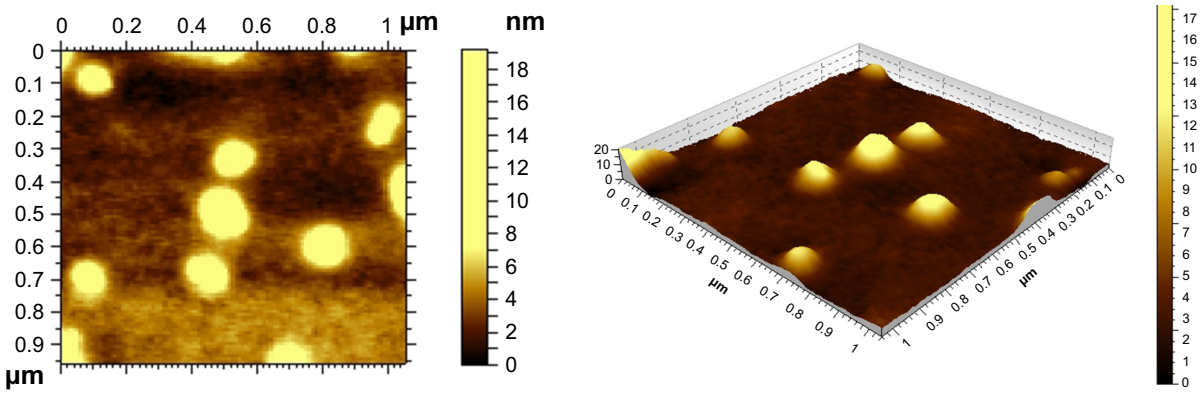

Figure S1 Atomic force microscopic images of CMCS-OH30 NP after the storage of 7 days at 4°C.
Abbreviation: CMCS-OH30 NP, carboxymethyl chitosan nanoparticles.

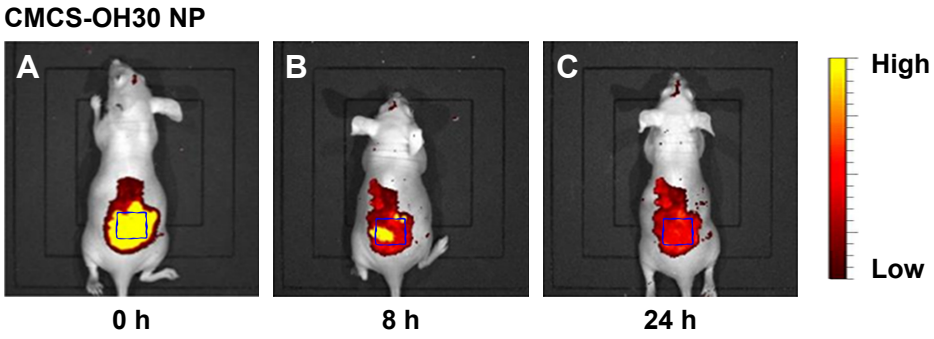

Figure S2 In vivo evaluation of controlled-releasing effects of prepared CMCS-OH30 NP.
Notes: Nanoparticles were prepared using FITC-labeled OH30. NIR optical imaging of nude mice at (**A**) 0 h, (**B**) 8 h, and (**C**) 24 h posttreatment.
Abbreviations: CMCS-OH30 NP, carboxymethyl chitosan nanoparticles; NIR, near-infrared.

International Journal of Nanomedicine

Dovepress

Publish your work in this journal

The International Journal of Nanomedicine is an international, peer-reviewed journal focusing on the application of nanotechnology in diagnostics, therapeutics, and drug delivery systems throughout the biomedical field. This journal is indexed on PubMed Central, MedLine, CAS, SciSearch®, Current Contents®/Clinical Medicine, Journal Citation Reports/Science Edition, EMBase, Scopus and the Elsevier Bibliographic databases. The manuscript management system is completely online and includes a very quick and fair peer-review system, which is all easy to use. Visit http://www.dovepress.com/testimonials.php to read real quotes from published authors.

Submit your manuscript here: http://www.dovepress.com/international-journal-of-nanomedicine-journal